AUTOMATED DETECTION OF STABLE FRACTURE POINTS IN COMPUTED TOMOGRAPHY IMAGE SEQUENCES

A.S. Chowdhury[1], S.M. Bhandarkar[1], G. Datta[2] and J.C. Yu[3, 4]
(ananda@cs.uga.edu, suchi@cs.uga.edu, gauri@stat.uga.edu, jyu@mcg.edu)

[1]Department of Computer Science
[2]Department of Statistics
The University of Georgia
Athens, Georgia 30602-7404, USA.

[3]Department of Plastic Surgery
[4]Dept. of Oral & Maxillofacial Surgery
The Medical College of Georgia
Augusta, Georgia 30912-4080, USA.

ABSTRACT

Automated detection of stable fracture points in a sequence of Computed Tomography (CT) images is found to be a challenging task. In this paper, an innovative scheme for automatic fracture detection in CT images is presented. The input to the system is a sequence of CT image slices of a fractured human mandible. Techniques from the curvature scale-space theory and graph based filtering (using prior anatomical knowledge) to first detect candidate fracture points in the individual CT slices. Subsequently, a Kalman filter incorporating a Bayesian perspective is used for testing the consistency of the candidate fracture points across all the CT slices in a given sequence. For the purpose of checking statistical consistency, both 95% and 99% high posterior density (HPD) prediction intervals are constructed. A spatial consistency term is coined for each candidate fracture point in terms of the number of slices in the CT image sequence, the number of times a fracture point detected in that sequence and the number of times it is found to be statistically consistent. Fracture points with spatial consistency terms close to unity are deemed to be stable fracture points for the CT image sequence under consideration.

Keywords: Curvature scale space, Graph-based filtering, Kalman filter, Bayesian statistics, Spatial consistency, Computed Tomography.

1. MOTIVATION

Introducing automation in various aspects of reconstructive surgery is a highly demanding and technically challenging task [1-2]. In the present work, we employ techniques from various diverse disciplines such as computer vision, graph theory and statistics to automatically detect stable fracture points in CT image sequences of a fractured human mandible. This constitutes a crucial and integral part of our larger virtual craniofacial reconstruction scheme [3]. The fracture surface data, which constitute the input to our virtual reconstruction algorithms, were thus far extracted with surgeons manually identifying the stable fracture points in the CT image sequence. This proved to be a performance bottleneck in the overall virtual reconstruction process, especially when dealing with complex multiple fractures. The proposed scheme automates the detection of stable fracture points and improves the speed and accuracy of the overall virtual craniofacial reconstruction.

2. IMAGE PRE-PROCESSING

The input to the system (Fig.1) is a sequence of two dimensional (2D) grayscale images of a fractured human mandible, generated via CT. Each image slice is 150 mm x 150 mm with an 8-bit color depth. A simple thresholding scheme is used to binarize each CT image slice (Fig. 2b). A 2D Connected Component Labeling (CCL) algorithm in conjunction with an area filter is used to remove some unwanted artifacts (Fig. 2c). The results of the 2D CCL algorithm are propagated across the CT image slices, resulting in a 3D CCL algorithm. Finally, a contour detection algorithm is applied to the individual bone fragments, identified as distinct components by the CCL algorithm, in all the CT image slices.

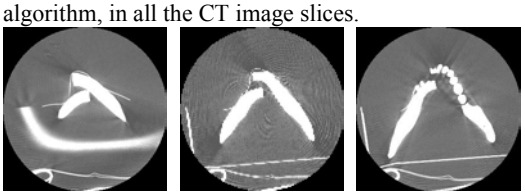

Fig.1: A typical sequence of 2D CT Images

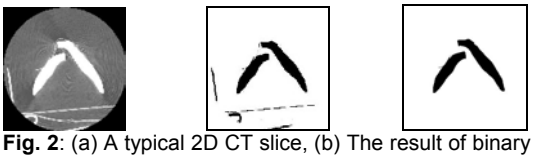

Fig. 2: (a) A typical 2D CT slice, (b) The result of binary thresholding on (a) and (c) The result of CCL and size filtering on (b).

3. FRACTURE POINT DETECTION IN INDIVIDUAL 2D SLICES

We used simple but useful concepts from curvature scale-space theory and graph theory to detect fracture points, which are essentially corners or points of high curvature [4-5] in the individual 2D CT image slices.

3.1 Generation of the initial pool of candidate fracture points

Let $|EL|$ be the total number of edge pixels of a component in any 2D CT slice where each edge pixel is represented as a 2D array element $EL[i]$, having coordinates $EL[i].x$ and $EL[i].y$. Let k be the number

of forward and backward edge pixels used to determine whether or not pixel i is a potential corner; φ_{ij} the angle between any two edge pixels i and j; and θ the threshold angle for corner determination. The following algorithm, based on curvature scale space theory, is used to determine a potential corner [4]:

for i: 1 -> |EL|
 for m: 1 -> k
 Find

$$\varphi_{i+m,i-m} = \tan^{-1}\left(\frac{EL[i+m].y - EL[i-m].y}{EL[i+m].x - EL[i-m].x}\right);$$

 end for;
 if $\forall$ m, $(|\varphi_{i+m,i-m}| > \theta)$
 mark pixel i as a potential fracture point;
 end if;
end for;

The complexity of the algorithm is $O(c \cdot k \cdot |EL|)$, where c is the number of components.

3.2 Graph-based filtering

With the corner points as vertices and the edges between vertices weighted by the Euclidean distance between them, an undirected weighted graph, denoted by $G = G(V, E)$ is constructed [5]. Listed below are the properties of G:

(1) $|V|$ is the initial set of corners obtained using curvature scale-space theory. Thus each vertex is essentially a point in the 2D space.

(2) The edges are deemed to exist only between successive vertices i.e. $|E| = |V| - 1$.

(3) The edge weights are given by the Euclidean distances ($\|\ \|$) between the corresponding vertices:

$$E[i][j] = \begin{cases} \|V_i - V_j\| & j = (i\%|V|)+1 \\ 0 & otherwise \end{cases} \quad (1)$$

where % denotes the integer division operator.

3.2.1 Vertex Condensation

If two vertices are very close in the constructed graph, then from prior anatomical knowledge we conclude that they cannot form the starting and terminating points of the fracture. So, a subgraph $G_1=G_1(V_1, E_1)$ is constructed. The complexity of the condensation process is $O(|E|)$. As the contours of a component under consideration can only be traced digitally, the chance of incurring error in the computation of the angle as well as the distance between two close vertices (as in Section 3.2.2) can be quite large. Thus the vertex condensation part, which coalesces two closely spaced vertices, before distance and/or angle computation, provides more accuracy.

3.2.2 Edge Validation

All the edges of the subgraph G_1 are checked and only those edges which satisfy the following two constraints are retained:

(a) The absolute value of the angle φ_{ij} between the two vertices i and j, given by:

$$\varphi_{ij} = \tan^{-1}\left(\frac{V_1[i].y - V_1[j].y}{V_1[i].x - V_1[j].x}\right) \quad (2)$$

is constrained to lie within a prespecified range:

$$\varphi_{ij} \in [\varphi_{\min},\ \varphi_{\max}] \quad (3)$$

b) The edge weight $E_1[i][j]$, which is the Euclidean distance between two vertices i and j, is constrained to lie within a prespecified range:

$$E_1[i][j] \in [l_{\min},\ l_{\max}] \quad (4)$$

From prior anatomical knowledge of the fracture edge lengths and orientations, all of $\varphi_{\min}$, $\varphi_{\max}$, l_{min}, l_{max} can be determined. Computation of φ_{ij}, $E_1[i][j]$ and checking their bounds can be performed individually in $O(1)$ time. Since this has to be done for each edge in G_1, the total complexity of this part is $O(|E_1|)$ and that of the entire graph based filtering is $O(|E|) + O(|E_1|)$, which is linear in the number of edges. The overall complexity of the two-phase corner detection process (using curvature scale-space theory and graph theory) for each CT slice is given by:

$$O(c.k.|EL|) + O(|E|) + O(|E_1|). \quad (5)$$

4. CHECKING FRACTURE POINT CONSISTENCY

Successive 2D CT slices of a given 3D object can be considered as being observed at successive timestamps. The goal is to track the various fracture points along successive 2D CT slices and develop a mathematical notion of spatial consistency.

4.1 Kalman filter with a Bayesian perspective

The basic measurement and state equations at time t are given by the following linear stochastic difference equations respectively [6]:

$$X_t = AX_{t-1} + w_t \quad (6)$$

$$Z_t = HX_t + v_t \quad (7)$$

where $X_t \in \Re^2$ is the actual state or parameter vector, $Z_t \in \Re^2$ is the measurement or observation of the velocity or (rate of) change of position of a fracture point in successive CT image slices. We assume both the process noise (w_t) and measurement noise (v_t) to be normally distributed with zero mean and constant variance Q and R respectively i.e.

$$p(w) \sim N(0, Q) \quad (8)$$

$$p(v) \sim N(0, R) \quad (9)$$

We further assumed that the estimation/prediction of the velocity/change in position along both the axes is mutually independent. Thus for our case, Q and R matrices are diagonal 2 x 2 matrices. Additionally, we assume A and H to be 2 x 2 identity matrices. Under the assumption that the initial state vector X is normal with mean μ_0 and variance Σ_0, we define:

$$\mu_{t-1} = E[X_{t-1} \mid \hat{Z}_{t-1}] \quad (10a)$$

$$\Sigma_{t-1} = \mathrm{var}[X_{t-1} \mid \hat{Z}_{t-1}] \quad (10b)$$

$$\hat{Z}_{t-1} = [Z_1, ..., Z_{t-1}] \quad (11)$$

Using equations (6)-(11) at any time *t*, the distribution of the state vector is normal with parameters [7-8]:

$$E[X_t \mid \hat{Z}_{t-1}] = \mu_{t-1} \quad (12a)$$

$$\text{var}[X_t \mid \hat{Z}_{t-1}] = \Sigma_{t-1} + Q \quad (12b)$$

The expected new observation has a normal distribution, with parameters:

$$E[Z_t \mid \hat{Z}_{t-1}] = \mu_{t-1} \quad (13a)$$

$$\text{var}[Z_t \mid \hat{Z}_{t-1}] = \Sigma_{t-1} + Q + R \quad (13b)$$

When a new observation Z_t is made, the parameter vector X_t is updated according to the Bayes' rule:

$$p(X_t \mid \hat{Z}_t) \propto p(Z_t \mid X_t)\, p(X_t \mid \hat{Z}_{t-1}) \quad (14)$$

Thus the posterior is normal with parameters:

$$E[X_t \mid \hat{Z}_t] = \mu_{t-1} + KF_t(Z_t - \mu_{t-1}) \quad (15a)$$

$$\text{var}[X_t \mid \hat{Z}_t] = (\Sigma_{t-1} + Q)(\Sigma_{t-1} + Q + R)^{-1} R \quad (15b)$$

where the Kalman Filter Gain KF_t at time *t* is given by:

$$KF_t = (\Sigma_t + Q)(\Sigma_t + Q + R)^{-1} \quad (16)$$

4.2 Stability and spatial consistency of fracture points

The spatial consistency for a particular fracture point is first checked in individual CT image slices (starting with the second slice). For this purpose, a high posterior density (HPD) prediction interval is constructed for the posterior distribution [9]. Since the HPD prediction interval needs to be developed at the same level of statistical significance α, for two independent directions *x* and *y*, Bonferroni's procedure is employed to detect the actual level of significance [10]. This is given by:

$$\alpha' = \alpha / 2 \quad (17)$$

The two-sided $100(1-\alpha)\%$ HPD prediction interval for the *x* and *y* directions are respectively given by [9]:

$$E[X_{1t} \mid \hat{Z}_{1t}] \pm (z_{\alpha'/2} * \sqrt{(\text{var}[X_{1t} \mid \hat{Z}_{1t}]) + R_{11}}) \quad (18)$$

$$E[X_{2t} \mid \hat{Z}_{2t}] \pm (z_{\alpha'/2} * \sqrt{(\text{var}[X_{2t} \mid \hat{Z}_{2t}]) + R_{22}}) \quad (19)$$

where the value of $z_{\alpha'/2}$ can be obtained from the standard normal table. Let the HPD prediction intervals at any time instance *t+1* along the two directions be HPD_{1t} and HPD_{2t} and the corresponding observations be Z_{1t+1} and Z_{2t+1} respectively. Then a fracture point is deemed as spatially consistent at time point *(t+1)* if the following condition is satisfied:

$$Z_{1t+1} \in HPD_{1t} \quad and \quad Z_{2t+1} \in HPD_{2t} \quad (20)$$

Each time instant in the present context actually corresponds to a CT image slice in a given CT image sequence. A particular fracture corner is deemed as stable or spatially consistent for a given image sequence, if it is detected as well as found to be spatially consistent for most of the slices in the sequence. Let *n* be the total number of slices in a given image sequence, *m* be the number of slices in which a particular fracture point is observed and *p* be the number of slices in which the fracture point is found to be spatially consistent. Then, we introduce a new term *S* as a measure of stability or spatial consistency for the entire image sequence:

$$S = 0.5 * ((m/n) + (p/n - 1)) \quad (21)$$

The maximum value of *S* is 1. So, a fracture point having a value of *S* very close to unity is deemed as a stable fracture point for the given CT image sequence.

5. EXPERIMENTAL RESULTS

A total of 472 potential fracture points were obtained using traditional curvature scale-space theory. By applying the first round of filtering, based on vertex condensation, 53% of the potential fracture points were eliminated (Table 1). In the second phase of filtering using edge length and edge orientation, a further 49% (approximately) of the potential fracture points were eliminated (Table 1). This can be seen in the first 3 rows of Fig. 3. In order to finally locate the stable or spatially consistent corners, we observed at most 6 fracture points to appear consistently across various the CT slices. This observation was based on the definition of spatial consistency (equation (20)) for an individual fracture point in a particular CT slice. Interestingly, not all the 6 fracture points were observed to be anatomically correct. Finally, the stability measure (equation (21)) was used to determine the stable fracture points for the given CT image sequence. The corners were enumerated from 1 to 6 from left to right and top to bottom in a 2D CT image slice. The first 4 corners were deemed to be stable for the given CT image sequence as they yielded values of *S* close to unity using 99% and 95% HPD prediction intervals (Table 2 and Table 3).

TABLE 1. Total number of fracture points obtained across all the 2D CT slices in a given image sequence by applying various techniques

Scheme	# of fracture points
Curvature Scale-space	472
Vertex Condensation	250
Edge-based filtering	123

TABLE 2. Value of *S* for the first 6 potential corners for a given CT image sequence using a 99% *HPD* prediction interval.

Corner No.	S (from equation 21)
1	0.93
2	0.92
3	0.85
4	0.84
5	0.05
6	0.05

TABLE 3. Value of *S* for the first 6 potential corners for a given CT image sequence using a 95% *HPD* prediction interval.

Corner No.	S (from equation 21)
1	0.90
2	0.90
3	0.85
4	0.82
5	0.05
6	0.05

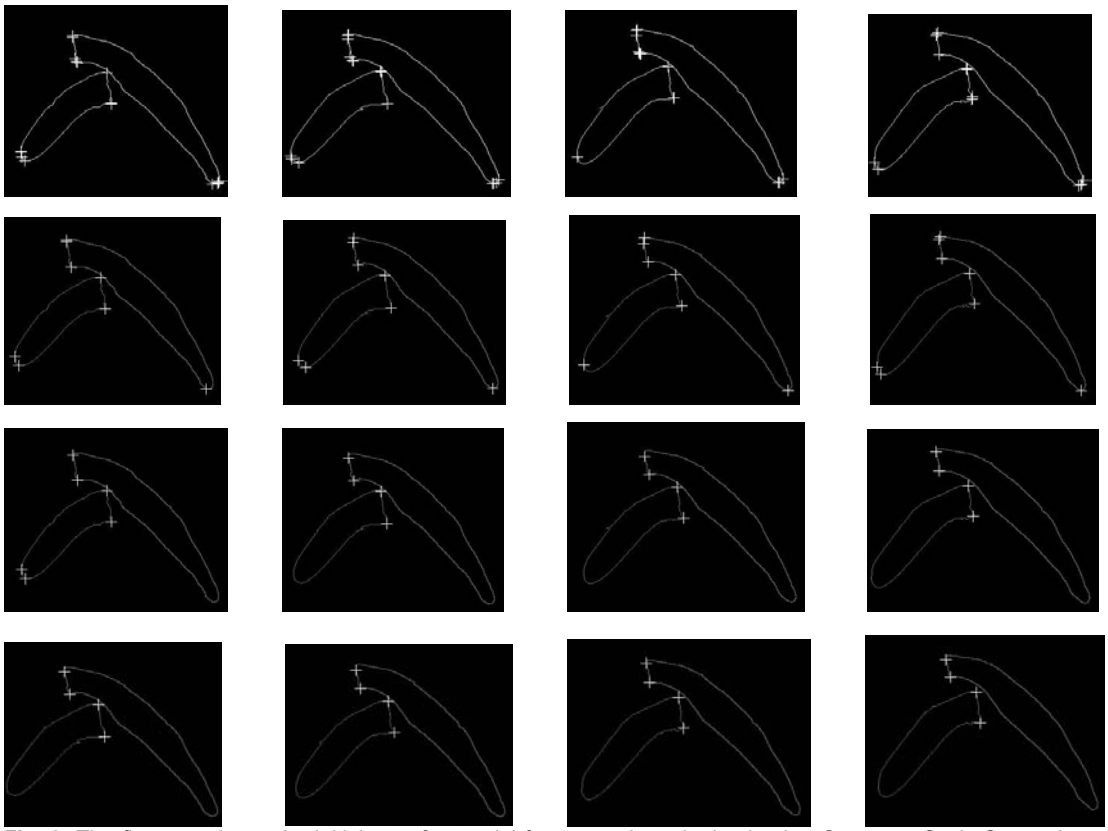

Fig. 3: The first row shows the initial set of potential fracture points obtained using Curvature Scale-Space theory; the second row shows the filtered fracture points using vertex condensation; the third row shows the further filtered fracture points using edge validation; the last row shows the stable fracture points obtained via Kalman filtering and application of the spatial consistency constraint in 4 successive CT slices.

6. CONCLUSIONS AND FUTURE WORK

An innovative and computationally efficient (quadratic-time) scheme, using techniques from computer vision, graph theory and statistics has been proposed for automated fracture point detection in a sequence of CT images of a fractured human mandible. An initial pool of potential fracture points is detected using traditional curvature scale-space theory. A two-step novel graph-based filtering technique that incorporates prior anatomical knowledge is employed to filter the initial set of potential fracture points. Finally, the stable fracture points for the given sequence are identified using Kalman filtering, construction of HPD prediction intervals, and the computation of an overall figure of merit. Future research will investigate a stricter bivariate analysis involving the Hoteling's T-transform instead of treating the x and y directions as two independent univariates [9] and the use of the Extended Kalman Filter and Particle Filter in more complex multi-fracture scenarios.

7. References

[1] T. Ozanian and R. Phillips, Image analysis for computer-assisted surgery of hip fractures, *Medical Image Analysis.* 4(2), 2000, pp. 137 - 159.

[2] S.E. Lim, Y. Xing, Y. Chen, W. Leow, T. Howe and M. Png, "Detection of Femur and Radius Fractures in X-ray images", *Proc. Intl. Conf. Medical Signal and Info. Process.,* Malta, G.C. 2004, pp. 1- 8.

[3] S.M. Bhandarkar, A.S. Chowdhury, Y. Tang, J. Yu and E.W. Tollner, Surface Matching Algorithms for Computer Aided Reconstructive Plastic Surgery, *Proc. IEEE Intl. Symp. Biomed. Imaging* (*ISBI)*, Arlington, VA, 2004, pp. 740 – 743.

[4] R. Jain, R. Kasturi and B. Schunck, *Machine Vision*. McGraw Hill, NY, 1995.

[5] D. Forsyth and J. Ponce, *Computer Vision A Modern Approach,* Prentice Hall, NJ, 2003.

[6] G. Welch and G. Bishop, *An Introduction to the Kalman Filter*, TR 95-041, UNC Chapel Hill, 2004.

[7] D. Pena and I. Gutman. Bayesian Approach to Robustifying the Kalman Filter, In Bayesian Analysis of Time Series And Dynamic Models, J. Spall (Ed.), Marcel Dekker, NY, 1988, pp. 227 – 253.

[8] R. Meinhold and N. Singpurwalla, "An article on the Kalman Filter", *The American Statistician*, 37(2), 1983, pp. 123- 127.

[9] Gelman A., Carlin J.B., Stern H.S. and D.B. Rubin, *Bayesian data Analysis*, Chapman & Hall/CRC, NY, 2004.

[10] Neter J., Kutner M., Wasserman W., Nachsteim C., *Applied Linear Statistical Models,* McGraw Hill, NY, 2002.